International Journal of Refrigeration 170 (2025) 468–476

Contents lists available at ScienceDirect

International Journal of Refrigeration

journal homepage: www.elsevier.com/locate/ijrefrig

INSTITUT INTERNATIONAL DU FROID
INTERNATIONAL INSTITUTE OF REFRIGERATION

Numerical simulation of active magnetic regenerative refrigeration using Gyroid structured regenerator at room temperature

Sotaro Nishioka *, Hossein Sepehri-Amin, Akiko T. Saito

National Institute for Materials Science, Ibaraki, 305-0003, Japan

ARTICLE INFO

Keywords:
Magnetic refrigeration
Triply periodic minimal surface
Gyroid
Regenerator
Heat transfer
CFD

ABSTRACT

The packed sphere bed regenerator is often utilized in active magnetic regenerative refrigeration (AMRR) because of its high heat transfer coefficient. However, the complex flow between the spheres in this regenerator causes an undesirable high pressure drop. In this study, we propose to adopt the Gyroid structure as a regenerator, which has a more structural design flexibility and a smoother flow, resulting in a lower pressure drop. The basic characteristics of various Gyroid regenerators were investigated by numerical simulations taking into account of heat transfer coefficient, pressure drop, and thermal conductivity, for the purpose of applying such regenerator in the AMRR system. The result of AMRR simulation shows that the standard Gyroid regenerator reduces the pressure drop by 45% while maintaining the cooling performance. In addition, two modified Gyroid regenerators have succeeded in further reducing the pressure drop with small decrease in cooling performance. This study shows that the Gyroid regenerator can serve as a potential regenerator to improve the energy efficiency of the AMRR system.

1. Introduction

Active magnetic regenerative refrigeration (AMRR) is a type of magnetic refrigeration which is based on the magnetocaloric effect (MCE) (Barclay and Steyert, 1982). AMRR can be used in a wide temperature range from room temperature to cryogenic temperatures by implementing magnetocaloric materials, as a regenerator, which show a large MCE with a desired magnetic transition temperature. Recently, there is a growing interest in application of AMRR for propane, hydrogen and natural gas liquefaction because AMRR is expected to have a higher efficiency than that of conventional gas expansion refrigeration (Barclay et al., 2019, Kamiya et al., 2022, Archipley et al., 2022). The regenerator plays three main roles in AMRR; heat regeneration, heat exchange with heat transfer fluid, and heat generation based on MCE. Although there have been intensive studies on the development of magnetocaloric materials with a large and reversible MCE (Pecharsky et al., 2001, Fujieda et al., 2002, Campoy et al., 2006, Rowe and Tura, 2006, Zhang et al., 2018, Kim et al., 2021, Hamdani et al., 2020, Tang et al., 2022), there is room to improve the current understanding on the influence of the shape of regenerator material on the performance of AMRR. Common shapes of regenerator materials used in AMRR are plate, flake, and sphere (Barclay et al., 2019, Kamiya et al., 2022, Archipley et al., 2022, Bohigas et al., 2000, Vasile and Muller, 2006, Tušek et al., 2010, Engelbrecht et al., 2013, Tura et al., 2012, Lei et al., 2017, Aprea et al., 2017, Li et al., 2019, Azad et al., 2021) among which the most commonly used shape is spherical powder with a size of sub-millimeter. The shape of regenerator material is selected in terms of porosity, volumetric heat transfer coefficient, thermal conductivity along flow direction, and pressure drop.

In this study, we focus on Gyroid structure as a shape of AMRR regenerator material. This structure was founded in 1970 as one of triply periodic minimal surface (TPMS) (Schoen, 1970). It has been considered that various applications in different fields (Al-Ketan et al., 2017, Sun et al., 2020, Al-Ketan et al., 2021, Theisen et al., 2022, Naghavi et al., 2022) such as engineering and medical science. Especially, Gyroid structure has attracted a great attention because it has intrinsic two independent flow channels and serves as good heat exchanger (Reynolds et al., 2021, Attarzadeh et al., 2021, Iyer et al., 2022, Yeranee and Rao, 2022, Dixit et al., 2022, Khalil et al., 2022, Abdelqader et al., 2024). The report shows a ~55% increase in exchanger effectiveness compared to a thermodynamically equivalent, most-efficient, counter-flow heat exchanger at 1/10th of its size (Dixit et al., 2022). Recently, the development of additive manufacturing (AM), also known as 3D printing technology, has made it possible to produce regenerators with complex 3D shapes, such as the gyroid structure, that cannot be produced using

* Corresponding author.
E-mail address: nishioka.sotaro@nims.go.jp (S. Nishioka).

https://doi.org/10.1016/j.ijrefrig.2024.11.018
Received 27 August 2024; Received in revised form 18 October 2024; Accepted 11 November 2024
Available online 13 November 2024

Nomenclature

Roman

A_s (m^2) Heat transfer surface area
A_v (1/m) Specific surface area
a (mm) Lattice constant
B_0 (T) Magnetic field
C (J/K) Heat capacity
c_p (J/kg·K) Specific heat
D_h (m) Hydraulic diameter
D_p (m) Particle diameter
f (-) Friction factor
h ($W/m^2·K$) Heat transfer coefficient
h_V ($W/m^3·K$) Volumetric heat transfer coefficient
L (m) Regenerator length
Nu (-) Nusselt number
Pr (-) Prandtl number
ΔP (Pa) Pressure drop
Re (-) Reynolds number
T (K) Temperature
ΔT (K) Temperature span
t_G (m) Thickness of Gyroid-sheet
u_s (m/s) Superficial speed in regenerator
V (m^3) Full regenerator volume

Greek

α, β, γ (-) Period parameter
α_t (m^2/s) Thermal diffusivity
ε (-) Porosity
λ_G (W/m·K) Effective thermal conductivity of Gyroid
λ (W/m·K) Thermal conductivity
λ_{norm} (-) Normalized effective thermal conductivity
μ (Pa·s) Viscosity
ρ (kg/m^3) Density
For physical property value, subscript of *f* and *s* means fluid and solid, respectively.

conventional processing technologies. Previous studies suggest that the Gyroid regenerator has advantages over the conventional one in terms of high heat transfer coefficient and low pressure drop (Reynolds et al., 2021, Attarzadeh et al., 2021, Iyer et al., 2022, Yeranee and Rao, 2022, Dixit et al., 2022). In addition, the selection of porosity of this structure is unrestricted by adjusting the sheet thickness; this is important for AMRR to control the balance of heat capacity between regenerator and heat transfer fluid from the perspective of efficient heat transportation. There are also studies on application of AM fabricating other shapes of AMRR regenerator material (Wieland and Petzoldt, 2017, Mohamed et al., 2022, Díaz-García et al., 2022, Sun et al., 2023, Imaizumi et al., 2024).

In this paper, we report results of simulation of AMRR, and calculations of heat transfer coefficient, thermal conductivity and pressure drop of various types of Gyroid regenerators. In addition, experiment and simulation of AMRR using the packed sphere bed regenerator were carried out to compare their temperature spans. Overall, Gyroid regenerator which has a flexible structure design, has a lower pressure drop compared to that of the packed sphere bed regenerator at same volumetric heat transfer coefficient. It was found that the effective thermal conductivity of Gyroid regenerator is 77% of bulk sample at the same porosity. Another remarkable result of this work is that the designed Gyroid regenerator results in a 45% reduction in pressure drop while maintaining the temperature span in the AMRR simulation. In other words, the Gyroid regenerator has the potential to improve the energy efficiency of the AMRR compared to conventional packed sphere bed regenerator.

2. Experiments

2.1. Design of Gyroid regenerator

Packed sphere bed regenerator is often used in regenerative refrigerator because of its higher volumetric heat transfer coefficient than that of plate and pillar regenerator. However, the drawbacks of high pressure drop due to the complex flow in the space between the spheres, leading to obstacles in improving operation frequency and energy efficiency in AMRR system. Therefore, we propose a regenerator with Gyroid structure as a base with the aim to achieve both high volumetric heat transfer coefficient and low pressure drop. Moreover, in contrast to the packed bed regenerator, the Gyroid regenerator has an integrated structure, hence it is considered to have advantages in terms of durability and mechanical strength against vibration during operation.

Gyroid surface (Fig. 1) has a cubic crystal structure with a space group of $I4_132$ and approximately given by

$$g(\boldsymbol{r}) = \sin\left(\frac{2\pi\alpha}{a}x\right)\cos\left(\frac{2\pi\beta}{a}y\right) + \sin\left(\frac{2\pi\beta}{a}y\right)\cos\left(\frac{2\pi\gamma}{a}z\right) + \sin\left(\frac{2\pi\gamma}{a}z\right)\cos\left(\frac{2\pi\alpha}{a}x\right). \quad (1)$$

And two surfaces located at a distance of $\pm t_G/2$ from eq. (1) is expressed as

$$F[\boldsymbol{r}] = g\left[x \pm \frac{t_G}{2R}\frac{\partial g(\boldsymbol{r})}{\partial x}, y \pm \frac{t_G}{2R}\frac{\partial g(\boldsymbol{r})}{\partial y}, z \pm \frac{t_G}{2R}\frac{\partial g(\boldsymbol{r})}{\partial z}\right], \quad (2)$$

where $R = sqrt\left[\left(\frac{\partial g(\boldsymbol{r})}{\partial x}\right)^2 + \left(\frac{\partial g(\boldsymbol{r})}{\partial y}\right)^2 + \left(\frac{\partial g(\boldsymbol{r})}{\partial z}\right)^2\right]$,

a is a lattice constant and α, β and γ are period parameters. Hence, the Gyroid-sheet (G-sheet) is exhibited as a space between two surfaces from eq. (2). The regenerators of G-sheet networks with different parameters were prepared as listed in Table 1. The period parameter affects the aspect ratio of a unit cell (Fig. 2); in this study, the aspect ratio of the regenerator was fixed at x:y:z = 3:1:1 for all types of regenerators by adjusting the array of unit cells. In order to achieve a smoother flow of fluid, the period parameter of α was reduced to 0.5 and 0.33 where β and γ remained as 1. The regenerators with three lattice constants are similar to one another. It is noticed that the porosity of Gyroid regenerator with

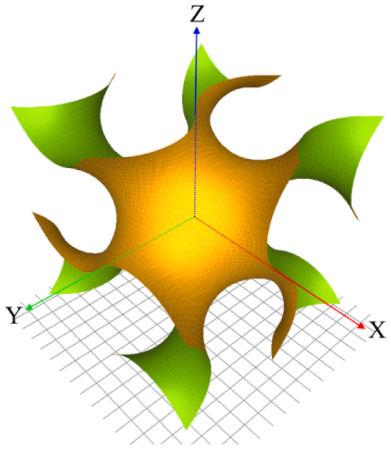

Fig. 1. Unit cell of Gyroid surface drawn from Eq. (1).

a relative thickness $t_G/a = 0.223$ is 0.361, which is very close to that of sphere packing. Fig. 2 (blue) shows the unit cell of G-sheet structure with a relative thickness $t_G/a = 0.223$. The specific surface area A_V was defined by heat transfer surface area A_s per full regenerator volume V, $A_V = A_s/V$. The effective thermal conductivity of Gyroid regenerator was calculated in section 3.2. And the normalized effective thermal conductivity is defined by $\lambda_{norm} = \lambda_G / \lambda_s(1 - \varepsilon)$.

Computational Fluid Dynamics (CFD) analyses were performed in a 3D for Gyroid regenerator, with parameters listed in Table 1, to calculate heat transfer coefficient h and pressure drop ΔP. The h was calculated from obtaining the temperature distribution of the fluid in the Gyroid regenerator (in section 3.1). The ΔP was defined as the pressure difference between both ends of the regenerator. The open source CFD software OpenFOAM (solver: rhoPimpleFoam) was used (Weller et al., 1998, Issa, 1986, Caretto et al., 1972) in this study. The calculation region is outside of G-sheet, in other words, the G-solid (also called G-bone) region. The conditions of CFD model for Gyroid regenerator are listed in Table 2. The meshes consisting of hexagonal elements, with a total mesh size of 14.4 - 15.5 million, is adequately large compared to previous research (Al-Ketan et al., 2021, Khalil et al., 2022, Abdelqader et al., 2024). Fig. 3 shows the meshed model of the G-solid networks with $t_G/a = 0.223$. Laminar flow was assumed based on the low Reynolds number Re (Reynolds et al., 2021, Attarzadeh et al., 2021, Iyer et al., 2022), expressed as

$$Re = \frac{\rho_f u_s D_h}{\varepsilon \mu} \quad \text{(for Gyroid)} \tag{3}$$

where ρ_f is density of fluid, μ is viscosity and ε is porosity of the regenerator. The hydraulic diameter in Gyroid structure (Reynolds et al., 2021, Iyer et al., 2022) is expressed as

$$D_h = \frac{4\varepsilon V}{A_s} \quad \text{(for Gyroid)} \tag{4}$$

where V, A_s and ε are full volume, heat transfer surface area and porosity of regenerators, respectively. The calculation of effective thermal conductivity of Gyroid regenerator was also performed in a 3D using OpenFOAM (solver: laplacianfoam) prior to the AMRR simulation.

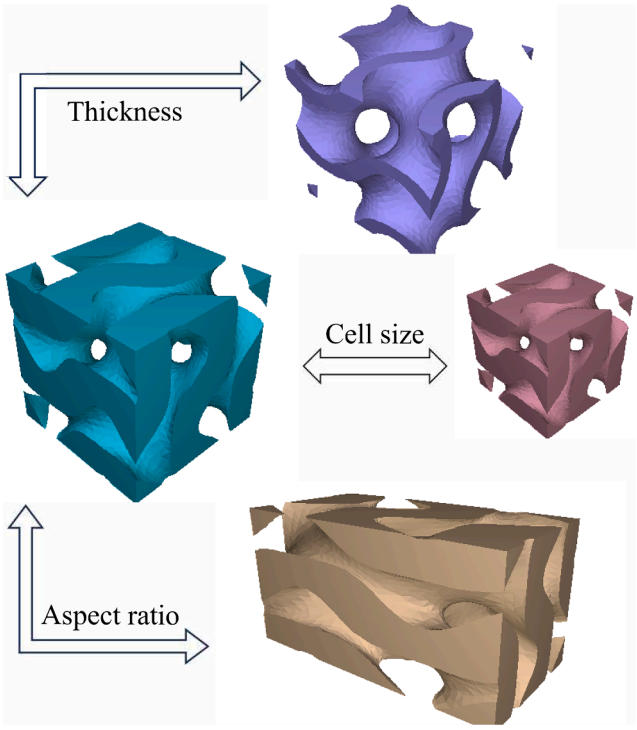

Fig. 2. 3D model of unit cell of standard Gyroid-sheet with $t_G/a = 0.223$ was shown in blue. The modified Gyroid-sheets used in this study were shown in other color. Click the 3D model in Adobe Acrobat Reader to activate the interactive 3D models. (Please see the supplementary material for 3D interactive image).

2.2. Design of AMRR system

Rotary type AMRR system was used in which magnetization and demagnetization are carried out by rotation of a double Halbach magnet. A schematic diagram and photograph of AMRR system are shown in

Table 1
Parameters of regenerator. The period parameter β and γ is 1 in this study.

Lattice constant a (mm)	Relative thickness t_G/a (-)	Porosity ε (-)	Period parameter α (-)	Array of unit cells $x \times y \times z$	Specific surface area A_v (1/m)	Normalized effective thermal conductivity λ_{norm} (-)	Symbol (Fig. 5)
1	0.191	0.557	1	9×3×3	5310	0.93	●
	0.223	0.361	1	9×3×3	4980	0.77	▲
			0.5	4.5×3×3	4280	0.90	■
			0.33	3×3×3	4120	0.95	◆
3.33	0.191	0.557	1	9×3×3	1590	0.93	●
	0.223	0.361	1	9×3×3	1490	0.77	▲
			0.5	4.5×3×3	1280	0.90	■
			0.33	3×3×3	1240	0.95	◆
10	0.191	0.557	1	9×3×3	531	0.93	●
	0.223	0.361	1	9×3×3	498	0.77	▲
			0.5	4.5×3×3	428	0.90	■
			0.33	3×3×3	412	0.95	◆

Table 2
CFD model for Gyroid regenerator.

Physics	Model
Dimension	3D simulation
Flow	Laminar
Time	Steady state
Fluid	Ethylene glycol solution (30 wt%)
Fluid prop.	Constant value for temperature
Flow speed (Boundary condition)	Inlet: 0.01 – 0.3 m/s (+X direction) Gyroid wall: No slip Side wall: No slip Outlet: Zero gradient
Temperature (Boundary condition)	Inlet: Fixed at 294 K Gyroid wall: Fixed at 304 K Side wall: Zero gradient Outlet: Zero gradient
Initial conditions	Flow speed: 0 m/s Temperature: 294 K
Mesh shape	Hexagonal
Mesh cells	14.4-15.5 million

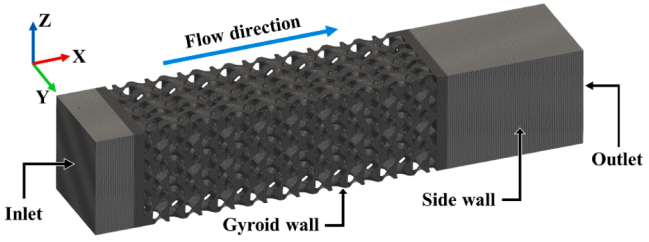

Fig. 3. Meshes of the G-solid networks (9×3×3 unit cells).

Fig. 4(a) and 4(b). The magnetic field of $B_0 = 1$ T with a gap of 20 mm is produced by double Halbach array of Nd-Fe-B magnets. Two platinum resistance thermometers (Pt100) are installed separately in the inlet and outlet tubes each and they are set 5 cm away from the high and low temperature ends of the regenerator. Spherical gadolinium was used as a magnetic refrigerant (regenerator material). The particle was fabricated by plasma rotating electrode process. Two sizes of particles, 350 - 500 μm and 500 - 600 μm, were extracted from the fabricated particles (Fig. 4(c)). The particles were packed in regenerator, and a porosity is ~0.37. The diameter and length of the regenerator is φ14 mm and 96 mm, respectively. Ethylene glycol solution (30 wt%) (Nybrine Z1 by Nisso Shoji co., LTD.) was used as the heat transfer fluid, which is flowed by continuous shuttle movement of the displacer. Fig. 4(d) shows the way the magnet and displacer are controlled for magnetization and demagnetization and heat transfer fluid flow, respectively. The time of one cycle of AMRR t_{cycle} is represented by $t_{cycle} = (t_M + t_{trans} + t_{wait} + t_D + t_{trans} + t_{wait})$ and is fixed at 2.4 sec; in other words, the operating frequency is 0.42 Hz. The typical parameters for the AMRR system are listed in Table 3. The physical properties of ethylene glycol solution (30 wt%) and gadolinium used in this study are shown in Table 4 (Bohne et al., 1984). CFD analyses were also performed for the system using OpenFOAM (solver: chtmultiregionfoam). Fig. 4(e) shows a cross-section view of axisymmetric 3D model used in the calculation, the calculation covers three regions of fluid (green), regenerator (yellow), as well as case and pipe (red).

2.3. Computational model

In this study, OpenFOAM solvers were used to obtain the temperature and pressure distribution of fluid region, where the continuity, momentum, and energy governing equations are presented using Einstein summation convention in Eqs. (5)-(7).

$$\frac{\partial \rho}{\partial t} + \frac{\partial (\rho u_i)}{\partial x_i} = 0, \tag{5}$$

$$\frac{\partial (\rho u_i)}{\partial t} + \frac{\partial (\rho u_i u_j)}{\partial x_j} = -\frac{\partial}{\partial x_i}\left(p + \frac{2}{3}\mu \frac{\partial u_j}{\partial x_j}\right) + \frac{\partial}{\partial x_j}\left[\mu\left(\frac{\partial u_i}{\partial x_j} + \frac{\partial u_j}{\partial x_i}\right)\right], \tag{6}$$

$$\frac{\partial (\rho H)}{\partial t} + \frac{\partial (\rho u_i H)}{\partial x_i} = \frac{\partial p}{\partial t} + \frac{\partial}{\partial x_i}\left(\lambda_f \frac{\partial T}{\partial x_i}\right) + \dot{q_f}, \tag{7}$$

where $H = h_e + K$, h_e is enthalpy, K is kinematic energy, $\dot{q_f}$ is the source term. On the other hands, the temperature distribution of solid regions such as Gyroid regenerator is calculated from Eq. (8),

$$\frac{\partial T}{\partial t} = \alpha_{ts} \Delta T + \dot{q_s}, \tag{8}$$

where α_{ts} is the thermal diffusivity and $\dot{q_s}$ is the source term. The amount of heat generation (or absorption) of the regenerator due to MCE, $\dot{q}_{MCE}$ is expressed in Eq. (9),

$$\dot{q}_{MCE} = \frac{1}{t_M} \int_0^{B_0} T \left(\frac{\partial M}{\partial T}\right)_B dB, \tag{9}$$

where t_M is the time required for applying magnetic field shown in Fig. 4 (d), and the effect is introduced into the calculation through a source term $\dot{q_s}$ in Eq. (8). The heat transfer between the fluid and solid regions is performed via the source term $\dot{q_F}$ and $\dot{q_s}$ each other using the parameter of heat transfer coefficient and specific surface area.

3. Results and Discussion

3.1. Fluid properties in regenerator

The pressure drop in packed sphere bed regenerator was measured using AMRR system (Fig. 4). Fig. 5(a) shows the calculated pressure drop per length for Gyroid structure with different lattice constant as a function of Reynolds number. The red, green, and blue lines are corresponding to Gyroid lattice constants of 1, 3.33, 10 mm. The black and gray lines represent experimentally measured data using packed sphere bed regenerator with particle diameters of ~550 and ~425 μm. The result of the measured pressure drop in packed sphere bed are close to that of calculated Gyroid regenerators with lattice constant of 1 mm. The pressure drop can be suppressed by adjusting α to a smaller value. As shown in Fig. 5(b), it is possible to clearly classify each regenerator structure design by using the friction factor f expressed by

$$f = \frac{\Delta P}{L} \frac{D_h}{\frac{1}{2}\rho_f \left(\frac{u_s}{\varepsilon}\right)^2}, \tag{10}$$

where hydraulic diameter D_h of packed bed expressed by

$$D_h = 6\frac{V_p}{A_p} = D_p \text{ (for packed sphere bed)}, \tag{11}$$

and D_h of Gyroid is shown in Eq. (4). Therefore, the pressure drop of Gyroid regenerator is inversely proportional to lattice constant. In each structure design, the change of the f became smaller with an increase in Re, which means that the inertia term proportional to the square of the velocity is dominant in the pressure drop (Fig. 5(b)).

The heat transfer coefficient of Gyroid regenerator was also calculated in a 3D steady state. The cross-section view of fluid temperature distribution in regenerator with $\varepsilon = 0.361$, $a = 1$ mm and $Re = 124$ ($u_s =$ 0.3 m/s) is shown in Fig. 6(Top) as an example of calculation. Fig. 6 (Bottom) shows several points of fluid temperature along flow direction (+X). The solid line is the fitting line used to obtain the heat transfer

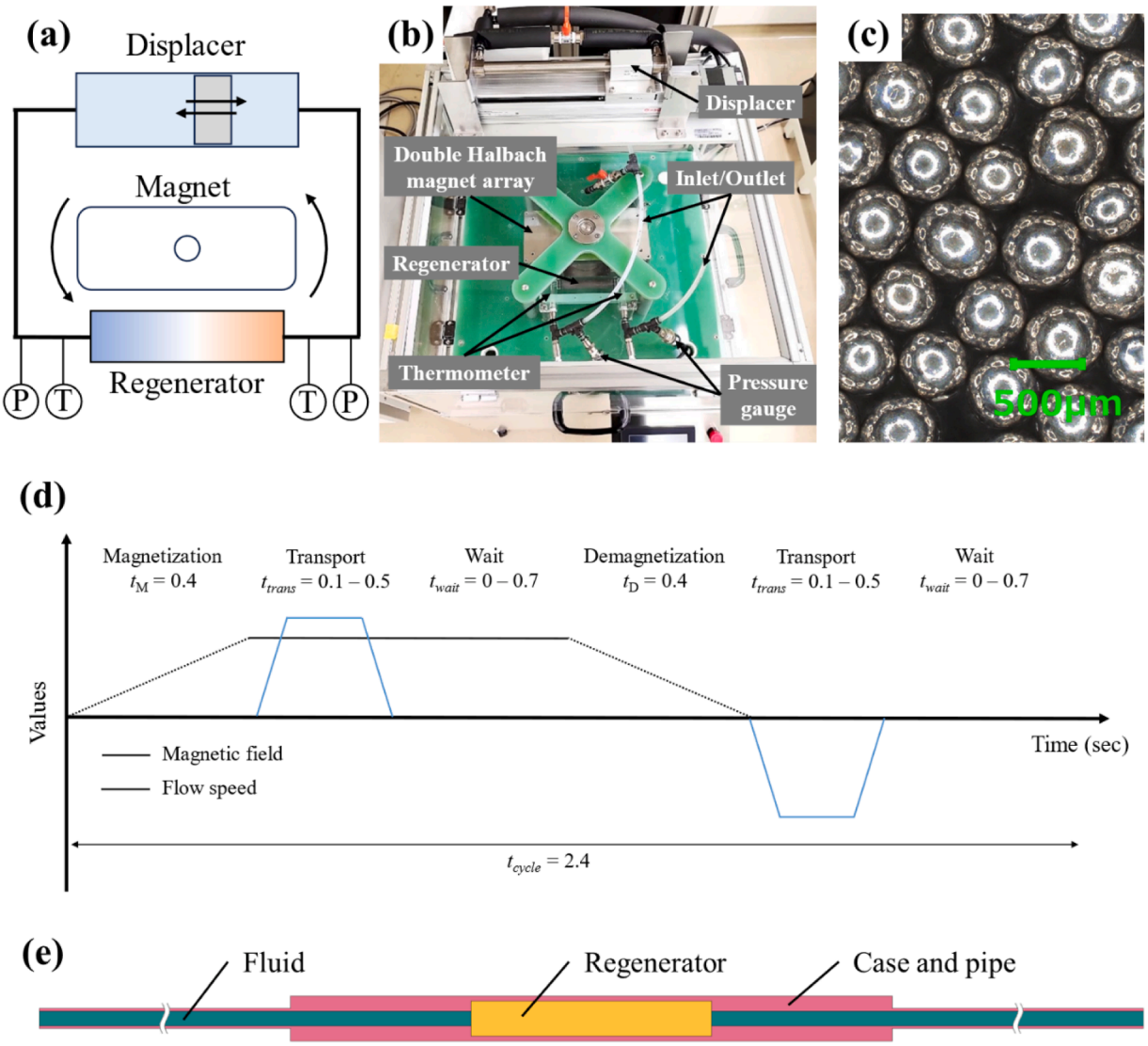

Fig. 4. (a) Schematic diagram of AMRR system. (b) Photograph of AMRR system. (c) Photograph of Gd particles with a size of 500 - 600 μm as a magnetic refrigerant. (d) Control procedure of AMRR in one cycle. (e) Cross-section view of axisymmetric 3D model used in the calculation. The calculation covers three regions which is fluid (green), regenerator (yellow), as well as case and pipe (red) regions.

coefficient h as expressed in the following equation,

$$dT(x) = \frac{dE}{C} = \frac{dQt}{c_{p_f}\rho_f\varphi t} = \frac{h(T_w - T(x))A_s}{c_{p_f}\rho_f\varphi L}dx$$
$$\therefore T(x) = T_w - (T_w - T_0)exp\left(-\frac{hA_s}{c_{p_f}\rho_f\varphi L}x\right), \quad (12)$$

where it considered that the heat energy received by the fluid at position x from the Gyroid regenerator wall in which temperature T_w is constant at 304 K. The calculations of volumetric heat transfer coefficient $h_V = h\,A_s/V$of regenerator with various parameters were performed. The amount of heat generation and absorption based on MCE depends on the volume of regenerator consists of magnetic material. Therefore, the h_V is useful for representing how quickly the heat by magnetocaloric effect is transferred to a fluid. In particular, it is necessary to use the h_V when comparing regenerators with different shapes, as their specific surface areas are different. The calculated h_V is shown in Fig. 5(c) as a function of *Re*. The overall result points out that the smaller the lattice constant, the lower the porosity and the more complex flows (higher α) giving rise to a higher h_v. The black and gray solid lines represent h_V of packed sphere bed regenerator of particle sizes of 550 and 425 μm were calculated by

$$h_V = \frac{A_s}{V}\frac{\lambda_f Nu}{D_h}, \quad (13)$$

where λ_f is the thermal conductivity of fluid (ethylene glycol solution), D_h is the hydraulic diameter shown in Eq. (11) and *Nu* is the Nusselt number, represented by (Frischmann et al., 2008)

$$Nu = 0.7Re^{0.60}Pr^{0.23}. \quad (14)$$

It is also shown that most of the values of h_v of the Gyroid regenerators with lattice constant of 1 mm remain higher than that of the packed sphere bed regenerator, while the values of $\Delta P/L$ of the Gyroid regenerators with the same lattice constant remain close and lower than that of the packed sphere bed regenerator. Based on the results of both $\Delta P/L$ and h_v, the Gyroid regenerator has the potential to outperform the conventional regenerators in AMRR. The Nusselt number of the Gyroid regenerator was calculated using calculated heat transfer coefficient as shown in Fig. 5(d). The black solid line was calculated using Eq. (14), and this equation is common to packed sphere bed regenerators. Also,

Table 3
Parameters of the AMRR system.

Item	Parameter	Value
AMRR	Type	Rotary
	Initial temperature	294 K
Magnetic subsystem	Magnet material	NdFeB
	Magnet dimension	100×70×30 mm
	Magnetic field	1 T
	Gap size	20 mm
Regenerator	Magnetocaloric material	Gd
	Geometry	Packed sphere bed
	Particle diameter	350 – 500 and 500 - 600 μm
	Regenerator dimension	φ14×96 mm
	Porosity	~0.37
Fluid circuit	Heat transfer fluid	Ethylene glycol solution (30 wt%)
	Flow volume	3.8 cm^3
	Superficial speed in regenerator	0.1 m/s
	Transport equipment	Displacer
Others	Operating frequency	0.42 Hz
Calculation	Dimension	3D simulation
	Flow	Laminar
	Time	Unsteady state
	Flow speed	Inlet and Outlet: ±0.1 m/s
	(Boundary condition)	Other: No slip
	Temperature	Outer wall of case and pipe: Fixed at 294 K
	(Boundary condition)	Inlet: Fixed at 294 K
		Outlet: Zero gradient
	Initial conditions	Flow speed: 0 m/s
		Temperature: 294 K
	Mesh shape	Hexagonal
	Mesh size	0.31 – 0.74 million

the Nusselt number can also clearly classify the heat transfer coefficient each regenerator structure design. Thus, the balance between pressure drop and heat transfer coefficient can be controlled not only by the lattice constant but also by the porosity and period parameter for each flow direction. The lower period parameter α expands the Gyroid cell along the flow direction (+X axis) and reduces the pressure drop at the expense of reducing the heat transfer coefficient, and vice versa. This design flexibility in the Gyroid structure serves as a significant advantage over the packed sphere bed regenerator, in which the sphere diameter and heat transfer coefficient are one-to-one linked.

3.2. Effective thermal conductivity of Gyroid regenerator

Effective thermal conductivity of Gyroid regenerator λ_G were calculated in a 3D steady state. The smaller effective thermal conductivity increases the insulation of the regenerator, resulting in a larger temperature difference between both ends of regenerator. Fig. 7(Top) shows the cross-section view of temperature distribution of regenerator with $t_G/a = 0.223$, $\varepsilon = 0.361$ and $\alpha = 0.5$ where temperature difference between both ends ΔT is set at 10 K. Fig. 6(Bottom) shows temperature change along X axis. The λ_G is obtained by equation below, a derivation from Fourier's law;

$$J = -\lambda_G \nabla T_G = -\lambda_s \nabla T_s = \frac{\Delta T}{\frac{L_G}{\lambda_G} + \frac{L_s}{\lambda_s}}, \ \therefore \lambda_G = -\frac{L_G}{\frac{\Delta T}{\nabla T_s} + L_s}\lambda_s, \tag{15}$$

where J is the heat flux,∇T_G and ∇T_s are temperature gradients of Gyroid area and solid ends, L_G and L_s are lengths of Gyroid area and solid ends, and λ_s is thermal conductivity of solid ends which is equal to that of bulk Gd. ∇T_s was obtained from the temperature distribution calculated where temperatures of both hot and cold ends were fixed at 304 K and 294 K, respectively (Fig. 7(Bottom)). The result shows ∇T_s = -161 K/m, therefore λ_G is 6.10 W/m K which is 90% of thermal conductivity of bulk Gd at the same porosity. For other Gyroid regenerators, the effective thermal conductivity is shown in Table 1. The trend of slight improvement in insulation has also been reported in previous papers (Luo et al., 2020).

3.3. AMRR simulation

The AMRR system (Fig. 4) was used to experimentally measure the temperature span. We used packed Gd sphere bed regenerator with particle diameters of ~550 μm (gray) and ~425 μm (black) (Fig. 8(a)). Moreover, we conducted simulations of the AMRR system with the same configuration as experiment (given parameters in Table 5) and plotted temperature span as shown in Fig. 8(b). The volumetric heat transfer coefficients calculated from Eq. (13) were used and substantially small value was assumed for the effective thermal conductivity of the regenerator. A comparison of experimental results and simulations on the saturated temperature span in AMR bed are in a good agreement (Fig. 8 (a) and 8(b)). In this simulation, the data of fluid temperature on a half cycle basis; therefore, the chattering occurred due to temperature oscillates. And the temperature spans at the center of the oscillation for particle diameters 550 μm and 425 μm are 12 K and 14 K, respectively.

AMRR simulation using Gyroid regenerators were also performed using the parameters shown in Table 5 under the same configuration. Fig. 8(c) shows the results of Gyroid regenerators of three period parameters α, 0.33 (yellow), 0.5 (blue) and 1 (red); their temperature spans are 10 K, 11 K and 14 K, respectively. Although the Gyroid regenerator exhibited a relatively high effective thermal conductivity as shown in Table 5, the results of AMRR simulation indicate that Gyroid regenerator property has little effect on temperature span; and this effect

Table 4
Physical properties. A magnetic property of Gadolinium was reported in previous report (Bjørk et al., 2010).

Material	$\rho\left(\frac{kg}{m^3}\right)$	$c_p\left(\frac{J}{kg \cdot K}\right)$	$\lambda\left(\frac{W}{m \cdot K}\right)$	μ (Pa·s)	Pr	$\alpha_t\left(\frac{m^2}{s}\right)$
Ethylene glycol solution (30 wt%)	1033	3800	0.46	0.002	16.5	1.17×10^{-7}
Gadolinium	7900	340	10.6	-	-	3.95×10^{-6}

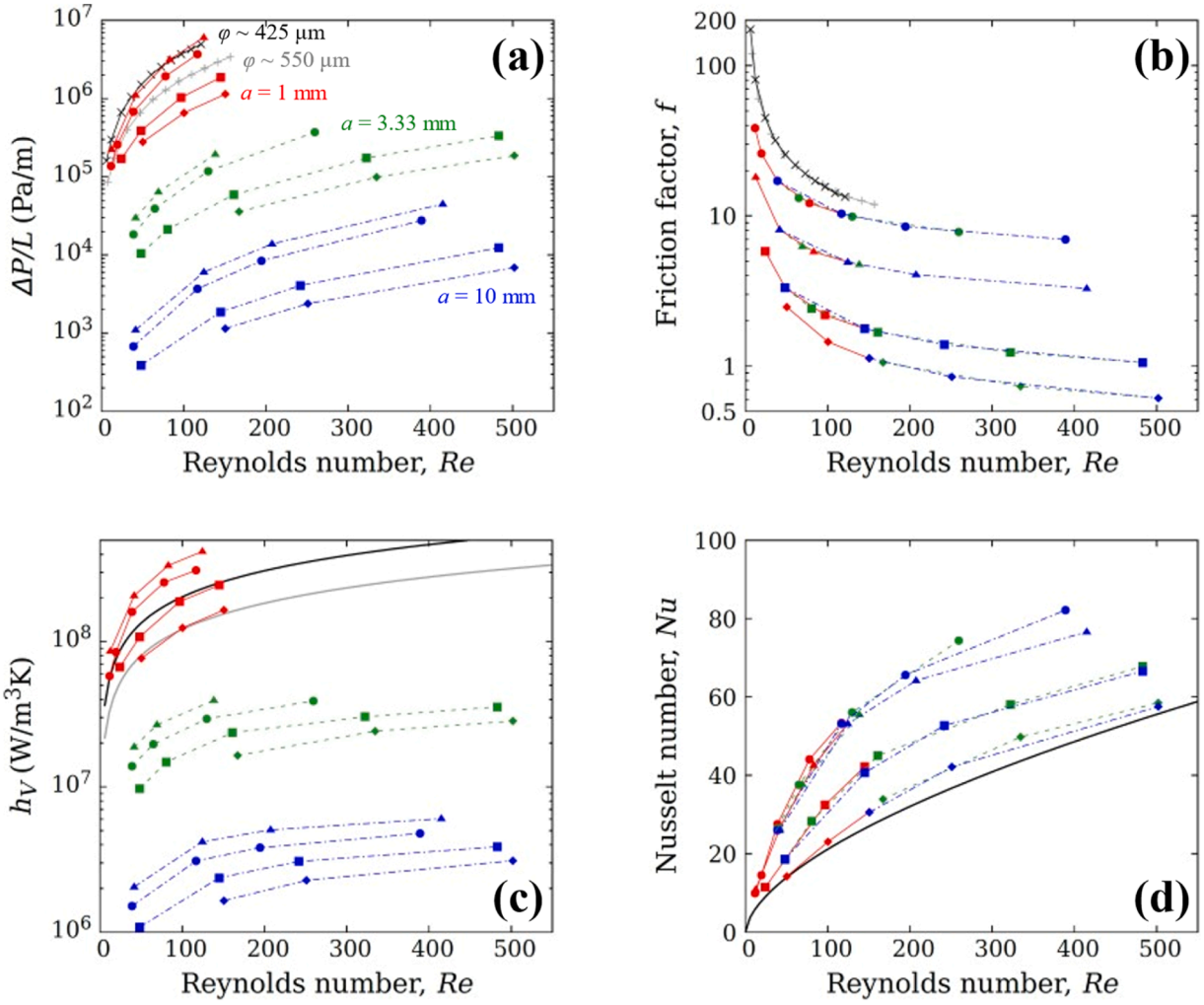

Fig. 5. Red, green, and blue lines are corresponding to Gyroid lattice constants of 1, 3.33, 10 mm. Black and gray lines represent measurement data using packed sphere bed regenerator of particle diameters of ~550 and ~425 μm. (a) Pressure drop per length. (b) Friction factor. (c) Volumetric heat transfer coefficient. (d) Nusselt number. Black solid line was calculated using Eq. (14), and this equation is common to packed sphere bed regenerators.

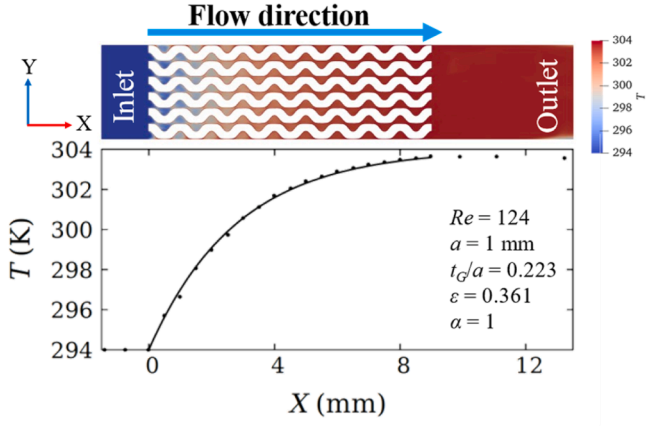

Fig. 6. (Top) Cross-section view of the temperature distribution of the fluid in the Gyroid regenerator. (Bottom) Points of fluid temperature in the regenerator along the flow direction. The regenerator parameters are $t_G/a = 0.223$, $\varepsilon = 0.361$, $\alpha = 1$, $a = 1$ mm and Reynolds number is $Re = 124$ ($u_s = 0.3$ m/s). The solid line is the fitting line used to obtain the heat transfer coefficient.

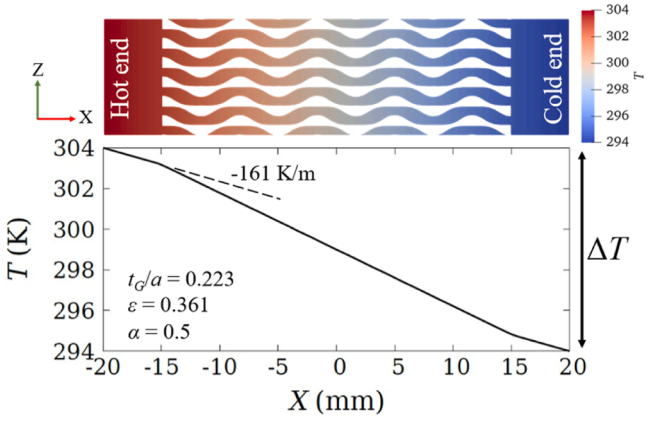

Fig. 7. (Top) Cross-section view of temperature distribution of Gyroid regenerator. (Bottom) The solid line represents temperature of the Gyroid regenerator along X axis. The dashed line represents temperature gradient of solid area ($\nabla T_s = -161$ K/m). The regenerator parameters are $t_G/a = 0.223$, $\varepsilon = 0.361$ and $\alpha = 0.5$. Temperatures of hot end and cold end are fixed at 304 K and 294 K, respectively.

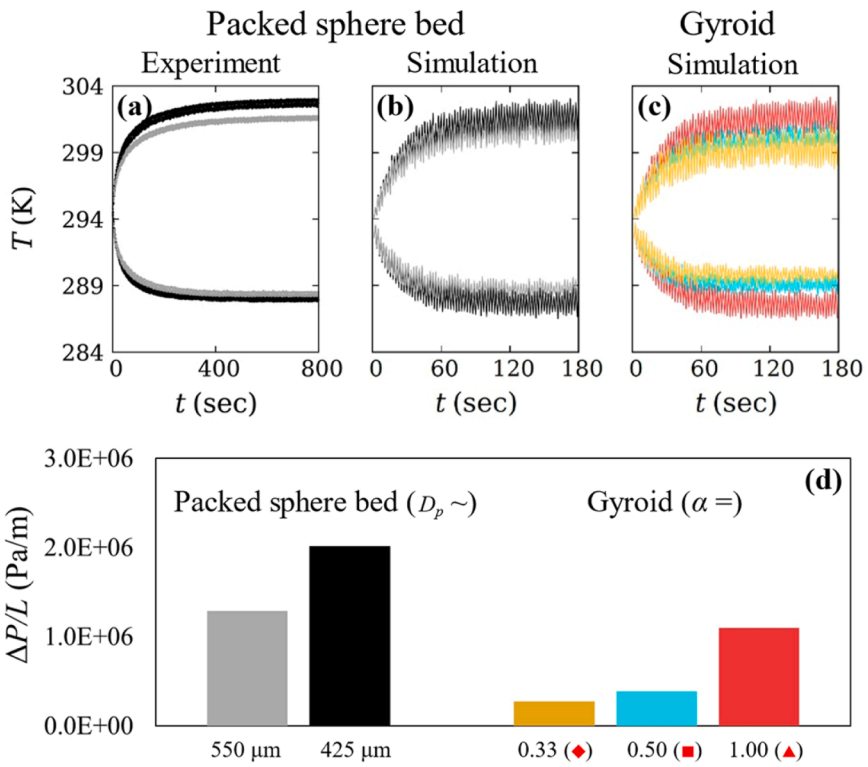

Fig. 8. Temperature change of fluid at location of thermometers; (a) display experiment and (b) simulation results for each half cycle of AMRR using packed Gd sphere bed regenerator, while (c) displays simulation result of Gyroid regenerator. (d) Pressure drop per regenerator length of packed sphere bed with two specified D_p by experiment, and three specified α of Gyroid by simulation; which is corresponding to (a), (b) and (c).

Table 5
Parameters of regenerator for AMRR simulation. The superficial speed in all regenerators is 0.1 m/s.

Type of regenerator	Packed sphere bed	Packed sphere bed	Gyroid (modified)	Gyroid (modified)	Gyroid (standard)
Symbol (Fig. 5)	+	×	◆	■	▲
Diameter D_p (μm)	550	425	-	-	-
Lattice constant a (mm)	-	-	1	1	1
Period parameter α (-)	-	-	0.33	0.5	1
Re (-)	78	61	50	48	41
h_v ($\times 10^6$ W/m^3·K)	105.8	151.8	76.54	107.5	207.2
$\Delta P/L$ ($\times 10^6$ Pa/m)	1.289	2.017	0.2787	0.3889	1.103
Effective λ (W/m·K)	0.10	0.10	6.42	6.10	5.22

becomes insignificant as operation frequency increases. The main reason for the different temperature spans of regenerators should be correlated to the difference in their volumetric heat transfer coefficients.

Fig. 8(d) shows the pressure drop of packed sphere bed regenerator with two specified D_p by experiment, and three specified α of Gyroid by simulation, which is corresponding to results of Fig. 8(a) and 8(c). At the same temperature span of 14 K, the standard Gyroid regenerator with $\alpha = 1$ reduced pressure drop by 45% compared to the packed sphere bed regenerator with $D_p \sim 425$ μm. In addition, the two modified Gyroid regenerators were able to reduce pressure drop by 80% (blue) and 86% (yellow) at the expense of only a small reduction in temperature range.

4. Summary

In this paper, the basic characteristics of the Gyroid regenerator, heat transfer coefficient, pressure drop, and thermal conductivity, were investigated using CFD analysis for the purpose of application in AMRR systems. In addition, AMRR simulations were performed to compare the cooling performance between the Gyroid regenerator and the conventional packed sphere bed regenerator. Result from the CFD analysis for the Gyroid regenerator with varied unit cell parameters (lattice constant, thickness and aspect ratio) shows that Gyroid regenerator has a lower pressure drop compared to that of the packed sphere bed regenerator at same volumetric heat transfer coefficient. It was also found that the heat transfer coefficient and pressure drop of all regenerators are characterized by the Nusselt number and friction factor. Although the Gyroid regenerator exhibited high effective thermal conductivity, which is 77-96% (depending on Gyroid shape) of bulk sample at same porosity; nevertheless, the results of AMRR simulation indicate that Gyroid regenerator property has little effect on temperature span. The overall CFD result of the standard Gyroid regenerator shows that the regenerator reduces pressure drop by 45% while maintaining the temperature span of 14 K, indicating improved energy efficiency. In addition, the two modified Gyroid regenerators could successfully reduce the pressure drop by 80% and 86% with the temperature span 11K and 10 K, respectively. We propose that the Gyroid regenerator with flexible design structure can serve as a potential regenerator to improve the energy efficiency and operation frequency of AMRR system.

CRediT authorship contribution statement

Sotaro Nishioka: Writing – original draft, Visualization, Software, Methodology, Investigation, Funding acquisition, Formal analysis, Data curation, Conceptualization. **Hossein Sepehri-Amin:** Writing – review & editing, Supervision, Resources, Funding acquisition, Conceptualization. **Akiko T. Saito:** Writing – review & editing, Supervision, Resources, Project administration, Funding acquisition, Formal analysis, Conceptualization.

Declaration of competing interest

The authors declare that they have no known competing financial interests or personal relationships that could have appeared to influence the work reported in this paper.

Acknowledgement

The authors were supported by the Hattori Hokokai Foundation (grant number 23-011) and the Kanamori Foundation. We would like to extend our gratitude to Dr. A. Uchida and Dr. H. Sebata for helping experiment. A special thanks to Dr. T. Hatano for the fruitful discussions. The calculations in this study were performed on the Numerical Materials Simulator at the NIMS.

Supplementary materials

Supplementary data associated with this article can be found, in the online version, at 10.1016/j.ijrefrig.2024.11.018.

Reference

J. A. Barclay and W. A. Steyert, “Active magnetic regenerator”, U.S. Patent 4,332,135 (1982).
Barclay, J., Brooks, K., Cui, J., Holladay, J., Meinhardt, K., Polikarpov, E., Thomsen, E., 2019. Cryogenics 100, 69–76. https://doi.org/10.1016/j.cryogenics.2019.01.009.
Kamiya, K., Matsumoto, K., Numazawa, T., Masuyama, S., Takeya, H., Saito, A.T., Kumazawa, N., Futatsuka, K., Matsunaga, K., Shirai, T., Takada, S., Iida, T., 2022. Appl. Phys. Express 15, 053001. https://doi.org/10.35848/1882-0786/ac5723.
Archipley, C., Barclay, J., Meinhardt, K., Whyatt, G., Thomsen, E., Holladay, J., Cui, J., Anderson, I., Wolf, S., 2022. Cryogenics 128, 103588. https://doi.org/10.1016/j.cryogenics.2022.103588.
Pecharsky, V.K., Gschneidner Jr., K.A., Pecharsky, A.O., Tishin, A.M., 2001. Phys. Rev. B 64, 144406. https://doi.org/10.1103/PhysRevB.64.144406.
Fujieda, S., Fujita, A., Fukamichi, K., 2002. Appl. Phys. Lett. 81, 1276–1278. https://doi.org/10.1063/1.1498148.
Campoy, J.C.P., Plaza, E.J.R., Coelho, A.A., Gama, S., 2006. Phys. Rev. B 74, 134410. https://doi.org/10.1103/PhysRevB.74.134410.
Rowe, A., Tura, A., 2006. Int. J. Refrig. 29, 1286–1293. https://doi.org/10.1016/j.ijrefrig.2006.07.012.
Zhang, X., Zhang, H., Qian, M., Geng, L., 2018. Sci. Rep. 8, 8235. https://doi.org/10.1038/s41598-018-26564-5.
Kim, E., Kang, K.H., Yoon, C.S., 2021. J. Magn. Magn. Mater. 530, 167952. https://doi.org/10.1016/j.jmmm.2021.167952.
Hamdani, K., Smaili, A., Sari, O., 2020. Renew. Energy 158, 487–499. https://doi.org/10.1016/j.renene.2020.05.149.
Tang, X., Sepehri-Amin, H., Terada, N., Martin-Cid, A., Kurniawan, I., Kobayashi, S., Kotani, Y., Takeya, H., Lai, J., Matsushita, Y., Ohkubo, T., Miura, Y., Nakamura, T., Hono, K., 2022. Nat. Commun. 13, 1817. https://doi.org/10.1038/s41467-022-29340-2.
Bohigas, X., Molins, E., Roig, A., Tejada, J., Zhang, X.X., 2000. IEEE Trans. Magn. 36, 538–544. https://doi.org/10.1109/20.846216.
Vasile, C., Muller, C., 2006. Int. J. Refrig. 29, 1318–1326. https://doi.org/10.1016/j.ijrefrig.2006.07.016.
Tušek, J., Zupan, S., Šarlah, A., Prebil, I., Poredoš, A., 2010. Int. J. Refrig. 33, 294–300. https://doi.org/10.1016/j.ijrefrig.2009.11.003.
Engelbrecht, K., Tušek, J., Nielsen, K.K., Kitanovski, A., Bahl, C.R.H., Poredoš, A., 2013. J. Phys. D: Appl. Phys. 46, 255002. https://doi.org/10.1088/0022-3727/46/25/255002.
Tura, A., Nielsen, K.K., Rowe, A., 2012. Int. J. Refrig. 35, 1518–1527. https://doi.org/10.1016/j.ijrefrig.2012.04.016.
Lei, T., Engelbrecht, K., Nielsen, K.K., Veje, C.T., 2017. Appl. Therm. Eng. 111, 1232–1243. https://doi.org/10.1016/j.applthermaleng.2015.11.113.
Aprea, C., Greco, A., Maiorino, A., Masselli, C., 2017. J. Phys.: Conf. Ser. 796, 012018. https://doi.org/10.1088/1742-6596/796/1/012018.
Li, Z., Shen, J., Li, K., Gao, X., Guo, X., Dai, W., 2019. Appl. Therm. Eng. 153, 159–167. https://doi.org/10.1016/j.applthermaleng.2019.02.100.
Azad, A., Ahmadi, P., Geshani, H., Wongwises, S., 2021. J. Therm. Anal. Calorim. 145, 1691–1710. https://doi.org/10.1007/s10973-021-10583-y.
Schoen, A.H., 1970. Technical Note NASA-TN-D-5541. NASA, Washington, DC.
Al-Ketan, O., Al-Rub, R.K.A., Rowshan, R., 2017. Adv. Mater. Technol. 2, 1600235. https://doi.org/10.1002/admt.201600235.
Sun, P., Wang, W., Zhang, W., Zhang, S., Gu, J., Yang, L., Pantelić, D., Jelenković, B., Zhang, D., 2020. ACS Appl. Mater. Interfaces 12, 34837–34847. https://doi.org/10.1021/acsami.0c06701.
Al-Ketan, O., Ali, M., Khalil, M., Rowshan, R., Khan, K.A., Al-Rub, R.K.A., 2021. J. Thermal Sci. Eng. Appl. 13 (2), 021010. https://doi.org/10.1115/1.4047385.
Theisen, A.-L., Lassmann, M., Tran-Gia, J., 2022. J. Nucl. Med. 63 (7), 1108–1116. https://doi.org/10.2967/jnumed.121.262925.
Naghavi, S.A., Tamaddon, M., Marghoub, A., Wang, K., Babamiri, B.B., Hazeli, K., Xu, W., Lu, X., Sun, C., Wang, L., Moazen, M., Wang, L., Li, D., Liu, C., 2022. Bioengineering 9 (10), 504. https://doi.org/10.3390/bioengineering9100504.
Reynolds, B.W., Fee, C.J., Morison, K.R., Holland, D.J., 2021. Int. J. Heat Mass Transf. 177, 121415. https://doi.org/10.1016/j.ijheatmasstransfer.2023.124264.
Attarzadeh, R., Rovira, M., Duwig, C., 2021. Int. J. Heat Mass Transf. 177, 121415. https://doi.org/10.1016/j.ijheatmasstransfer.2021.121415.
Iyer, J., Moore, T., Nguyen, D., Roy, P., Stolaroff, J., 2022. Appl. Therm. Eng. 209, 118192. https://doi.org/10.1016/j.applthermaleng.2022.118192.
Yeranee, K., Rao, Y., 2022. Energies 15 (23), 8994. https://doi.org/10.3390/en15238994.
Dixit, T., Al-Hajri, E., Paul, M.C, Nithiarasu, P., Kumar, S., 2022. Appl. Therm. Eng. 210, 118339. https://doi.org/10.1016/j.applthermaleng.2022.118339.
Khalil, M., Ali, M.I.H., Khan, K.A., Al-Rub, R.A., 2022. CaseStud. Therm. Eng. 38, 102313. https://doi.org/10.1016/j.csite.2022.102313.
Abdelqader, O., Al-Rub, R.K.A., Ali, M.I.H., 2024. Appl. Therm. Eng. 246, 122979. https://doi.org/10.1016/j.applthermaleng.2024.122979.
Wieland, S., Petzoldt, Frank, 2017. J. Alloys Compd. 719, 182–188. https://doi.org/10.1016/j.jallcom.2017.05.168.
Mohamed, A.E.-M.A., Jeong, M., Sheridan, R.S., Attallah, M.M., 2022. Addit. Manuf. 51, 102620. https://doi.org/10.1016/j.addma.2022.102620.
Díaz-García, Á., Revuelta, J., Moreno-Ramírez, L.M., Law, J.Y., Mayer, C., Franco, V., 2022. Compos. Commun. 35, 101352. https://doi.org/10.1016/j.coco.2022.101352.
Sun, K., Mohamed, A.E.-M.A., Li, S., Jeong, M., Head, J., Attallah, M.M., 2023. Addit. Manuf. 69, 103536. https://doi.org/10.1016/j.addma.2023.103536.
Imaizumi, K., Fujita, A., Suzuki, A., Kobashi, M., Kato, M., 2024. Addit. Manuf. 83, 104076. https://doi.org/10.1016/j.addma.2024.104076.
Weller, H.G., Tabor, G., Jasak, H., Fureby, C., 1998. Comput. Phys. 12, 620–631. https://doi.org/10.1063/1.168744.
Issa, R.I., 1986. J. Comput. Phys. 62 (1), 40–65. https://doi.org/10.1016/0021-9991(86)90099-9.
Caretto, L.S., Gosman, A.D., Patankar, S.V., Spalding, D.B., 1972. In: Proceedings of the Third International Conference on Numerical Methods in Fluid Mechanics, 19. Springer, pp. 60–68. https://doi.org/10.1007/BFb0112677 of Lecture Notes in Physics, pages.
Bohne, D., Fischer, S., Obermeier, E., 1984. Ber. Bunsenges. Phy. Chem 88 (8), 739–742. https://doi.org/10.1002/bbpc.19840880813.
Bjørk, R., Bahl, C.R.H., Katter, M., 2010. J. Magn. Magn. Mater. 322, 3882–3888. https://doi.org/10.1016/j.jmmm.2010.08.013.
Frischmann, M., Engelbercht, K., Nells, G., Klein, S., 2008. In: International refrigeration and air conditioning conference, p. 2326. http://docs.lib.purdue.edu/iracc/935.
Luo, J.-W., Chen, L., Min, T., Shan, F., Kang, Q., Tao, W.Q., 2020. Int. J. Heat Mass Transf. 146, 118837. https://doi.org/10.1016/j.ijheatmasstransfer.2019.118837.